Available online at www.sciencedirect.com
SCIENCE DIRECT®
Physics Reports 386 (2003) 1–27
PHYSICS REPORTS
www.elsevier.com/locate/physrep

Model-independent low momentum nucleon interaction from phase shift equivalence

S.K. Bogner[a,b,*], T.T.S. Kuo[b], A. Schwenk[c,b]

[a] *Institute for Nuclear Theory, Box 351550, University of Washington, Seattle, WA 98195, USA*
[b] *Department of Physics and Astronomy, State University of New York, Stony Brook, NY 11794-3800, USA*
[c] *Department of Physics, The Ohio State University, Columbus, OH 43210, USA*

Accepted 10 July 2003
editor: G.E. Brown

Abstract

We present detailed results for the model-independent low momentum nucleon–nucleon interaction $V_{\mathrm{low}\,k}$. By introducing a cutoff in momentum space, we separate the Hilbert space into a low momentum and a high momentum part. The renormalization group is used to construct the effective interaction $V_{\mathrm{low}\,k}$ in the low momentum space, starting from various high precision potential models commonly used in nuclear many-body calculations. With a cutoff in the range of $\Lambda \sim 2.1$ fm^{-1}, the new potential $V_{\mathrm{low}\,k}$ is independent of the input model, and reproduces the experimental phase shift data for corresponding laboratory energies below $E_{\mathrm{lab}} \sim 350$ MeV, as well as the deuteron binding energy with similar accuracy as the realistic input potentials. The model independence of $V_{\mathrm{low}\,k}$ demonstrates that the physics of nucleons interacting at low momenta does not depend on details of the high momentum dynamics assumed in conventional potential models. $V_{\mathrm{low}\,k}$ does not have momentum components larger than the cutoff, and as a consequence is considerably softer than the high precision potentials. Therefore, when $V_{\mathrm{low}\,k}$ is used as microscopic input in the many-body problem, the high momentum effects in the particle–particle channel do not have to be addressed by performing a Brueckner ladder resummation or short-range correlation methods. By varying the cutoff, we study how the model independence of $V_{\mathrm{low}\,k}$ is reached in different partial waves. This provides numerical evidence for the separation of scales in the nuclear problem, and physical insight into the nature of the low momentum interaction.

PACS: 13.75.Cs; 21.30. − x; 11.10.Hi

Keywords: Nucleon–nucleon interactions; Effective interactions; Renormalization group

* Corresponding author. Institute for Nuclear Theory, Box 351550, University of Washington, Seattle, WA 98195, USA.
E-mail addresses: bogner@phys.washington.edu (S.K. Bogner), kuo@nuclear.physics.sunysb.edu (T.T.S. Kuo), aschwenk@mps.ohio-state.edu (A. Schwenk).

0370-1573/$ - see front matter
doi:10.1016/j.physrep.2003.07.001

Contents

1. Introduction

A major challenge of nuclear physics lies in the description of finite nuclei and nuclear matter on the basis of a microscopic theory. By microscopic theory, it is understood that the input nuclear force is, as best as possible, based on the available free-space data, e.g., the elastic nucleon–nucleon and nucleon–deuteron scattering phase shifts. The theoretical predictions are then obtained using a systematic many-body approach, which is reliable for strongly interacting systems.

At low energies and densities, one typically starts by treating protons and neutrons as nonrelativistic point-like fermions. However, as opposed to the Coulomb interaction in electronic systems, the nucleon–nucleon interaction remains unknown from the underlying theory of the strong interactions, quantum chromodynamics (QCD). Thus, phenomenological meson-exchange models of the two-nucleon force are commonly used as input in many-body calculations. Moreover, three- (and possibly four-) body forces are needed to obtain accurate results for few-body systems. Recent Green's function Monte Carlo calculations using a realistic two-body interaction, the Argonne v_{18} potential, have shown that three-body forces typically contribute a net attraction of $\approx 20\%$ to the low-lying states of light nuclei, $A \leqslant 10$ [1,2].

However, already at the lowest level of the two-body interaction, there are several quite different potential models commonly used. Therefore, it is a natural first step to ask whether it is possible to remove or to minimize this model dependence. In this work, we expand on previous results [3,4] and demonstrate that this is indeed possible, as long as one restricts the interaction to momenta which are constrained by the experimental scattering data, and explicitly includes the long-range part of the interaction.

There are number of high precision models of the nucleon–nucleon force V_{NN}, which we will refer to as the "bare" interactions. All realistic potentials are given by the one-pion exchange (OPE) interaction at long distances, but vary substantially in their treatment of the intermediate-range attraction and the short-range repulsion. We briefly summarize the different frameworks used to generate the intermediate and short-range parts of the realistic potential models [5,6]. The Paris potential

[7] calculates the intermediate-range contributions to the nucleon–nucleon scattering amplitude from two-pion exchange using dispersion theory, and then assumes a local potential representation consisting of several static Yukawa functions. The ω-meson exchange at short distances is included as part of the three-pion exchange, and a repulsive core is introduced by sharply cutting off these parts at the internucleon distance $r \sim 0.8$ fm. At short distances, the interaction is simply given by a constant (but energy-dependent) soft core. The Bonn potentials [8] are based on multiple one-boson exchange interactions and the two-pion exchange potential calculated in perturbation theory. The two-pion exchange contribution is then approximated by an energy-independent σ-meson exchange term. Smooth form factors (with typical form factor masses $\approx$1–2 GeV) cut off the potential at short distances. The short-range repulsion originates from the ω exchange. The second generation CD-Bonn potential [9,10] refines the treatment of the one-boson exchange amplitudes to take into account the non-local structure arising from the covariant amplitudes. The Nijmegen potentials [11] consist of multiple one-boson exchange parts (with separate local and non-local versions), where the interaction parameters of the heavier mesons depend on the partial waves. At very short distances, the potentials are regularized by exponential form factors. Finally, the local Argonne potential [12] consists of the OPE interaction regularized at short distances, and a phenomenological parametrization at short and intermediate distances. The core is provided by Woods–Saxon functions that are effective at a distance $r \sim 0.5$ fm.

Over the past decade, there has also been a great effort in deriving low-energy nucleon–nucleon interactions in the framework of effective field theory (EFT) [13–19] (for a review see [20]). The EFT approach is based on local Lagrangian field theory with low-energy degrees of freedom, constrained by the symmetries of QCD. The Lagrangian contains the nucleon and pion fields and all possible interactions consistent with chiral symmetry. At low energies, the heavy mesons and nucleon resonances can be integrated out of the theory. Their effects are encoded in the renormalized pion exchange and scale-dependent coupling constants of model-independent contact interactions. By formulating a power counting scheme, the number of couplings in the effective Lagrangian can be truncated and fitted to a set of low-energy data. Once the low-energy couplings are determined, the power counting scheme enables the EFT to predict other processes with controlled error estimates.

In addition to the high precision phenomenological interactions, we study the Idaho potential [19], which is a chiral model inspired by EFT. The Idaho potential introduces some model dependence in contrast to the rigorous EFT interactions by, e.g., including several terms in the expansion which are subleading in the power counting with respect to omitted ones. This leads to a better description of the experimental phase shifts, comparable in accuracy to the realistic models. Since we will argue that our results are dependent on the accurate reproduction of the scattering phase shifts, the results for the Idaho EFT potential are presented here as well.

The couplings and parameters of the different potentials described above are fitted to the elastic nucleon–nucleon scattering phase shifts over laboratory energies $E_{\rm lab} \lesssim 350$ MeV and the low-energy deuteron properties. As a consequence, the bare interactions are constrained by the experimental data up to a corresponding relative momentum scale of[1]

$$\Lambda_{\rm data} \sim 2.1 \text{ fm}^{-1} \ . \tag{1}$$

[1] Here, we use conventional scattering units where $c = \hbar = \hbar^2/m = 1$, i.e., the laboratory energy is related to the relative momentum through $E_{\rm lab} = 2k^2$.

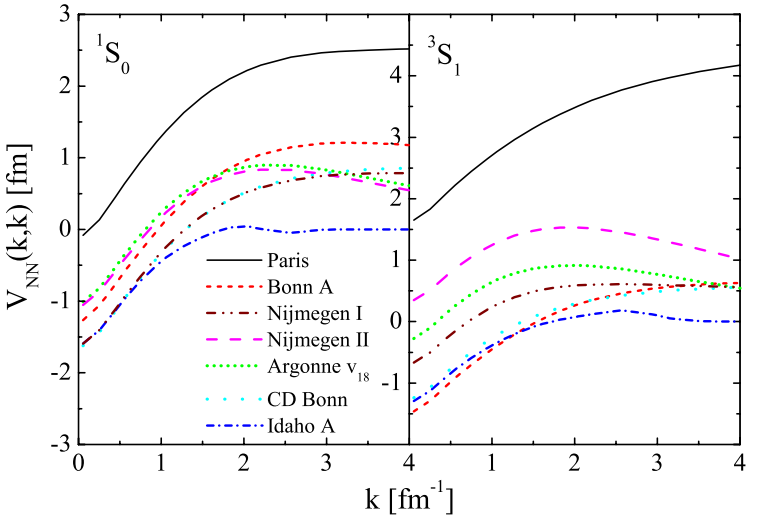

Fig. 1. The diagonal momentum-space matrix elements of the different high precision potentials $V_{\rm NN}$ versus relative momentum in the $^1S_0$ and $^3S_1$ partial wave.

This is manifest in Fig. 1, where we observe that various high precision potential models of $V_{\rm NN}$ have quite different momentum-space components, despite their common treatment of the OPE interaction and the reproduction of the same low-energy data. This indicates that the low-energy observables are not sensitive to the details or different assumptions of the short-distance physics. This insensitivity is a consequence of the separation of long- and short-distance scales in the nuclear force, and implies that the nucleon–nucleon interaction is amenable to an effective theory or renormalization group treatment.

1.1. The two-body problem in effective theories

In this work, we propose a renormalization group (RG) approach to the nucleon–nucleon interaction which removes the short-distance model dependencies of the high precision potentials, while preserving their high accuracy description of the nucleon–nucleon scattering data and deuteron properties. As our approach is a compromise between an EFT treatment and the high precision potentials, we first discuss in general terms how effective theory methods can be applied to the two-nucleon problem.

The fundamental principle underlying modern effective theory methods is simple: the low-energy physics is not sensitive to the details of the high-energy dynamics. In other words, one can construct arbitrarily many theories, which have the same long-wavelength structure and lead to identical low-energy observables, but differ at short distances and higher-energy scales. This ambiguity can be used constructively. Namely, it is possible to replace the detailed short-distance dynamics by simple effective interactions, which preserve the low-energy symmetries of the full theory.

For example, a forerunner to the modern EFT approach is the well-known effective range theory of Bethe and Longmire [21]. This allowed a quantitative description of low-energy nuclear phenomena without a detailed knowledge of the nuclear force. The low-energy scattering amplitude $T(k,k;k^2)$ is given by two phenomenological low-energy constants independent of an assumed nuclear force

model [22]

$$\frac{1}{T(k,k;k^2)} = \frac{1}{a_s} - \frac{1}{2} r_0 k^2 + \mathcal{O}(k^4) \ , \tag{2}$$

where a_s denotes the scattering length and r_0 is the effective range parameter. The effective range theory encompasses the fundamental principle of modern effective theories, as any force models with different short-distance details can be tuned to give the same low-energy physics, which is captured in the effective range parameters.

More generally, this insensitivity can be exploited when the short-distance dynamics are either poorly understood, or are too complicated for calculation. Consider a quantum system described by the Hamiltonian

$$H = H_0 + V_L + V_H \ , \tag{3}$$

where V_L primarily couples to low-energy states, in our case the long-range part of the OPE interaction, and V_H includes the remaining complicated or unknown short-distance part of the interaction.

A first step in building an effective theory is to impose a cutoff Λ on the intermediate state energies and momenta. In the modern viewpoint, the cutoff takes on a physical meaning. It divides the low-energy states, which are essential to the low-energy physics, from the high-energy modes. In this way, one explicitly maintains only dynamics that are well understood. It is, however, not possible to simply neglect the remaining V_H, since its effects on the low-energy physics need to be included in the form of correction, or so-called counterterms. The correction terms are constrained by demanding that all low-energy spectra, low-energy amplitudes, etc., calculated using the bare Hamiltonian H are exactly reproduced using an effective Hamiltonian $H_{\mathrm{low}\,k}$ in the truncated Hilbert space.

Schematically, in perturbation theory all amplitudes are of the form

$$\langle f|\mathscr{A}|i\rangle = \langle f|V_{\mathrm{bare}}|i\rangle + \sum_{n=0}^{\infty} \frac{\langle f|V_{\mathrm{bare}}|n\rangle\langle n|V_{\mathrm{bare}}|i\rangle}{E_i - E_n} + \mathcal{O}(V_{\mathrm{bare}}^3) \ , \tag{4}$$

where the intermediate state summations are over both low and high-energy states. We now define an effective low momentum potential $V_{\mathrm{low}\,k}$ by demanding

$$\langle f|\mathscr{A}|i\rangle = \langle f|V_{\mathrm{low}\,k}|i\rangle + \sum_{n=0}^{\Lambda} \frac{\langle f|V_{\mathrm{low}\,k}|n\rangle\langle n|V_{\mathrm{low}\,k}|i\rangle}{E_i - E_n} + \mathcal{O}(V_{\mathrm{low}\,k}^3) \ , \tag{5}$$

where we introduce the correction terms through

$$V_{\mathrm{low}\,k} = V_L + \delta V_{\mathrm{ct}} \ . \tag{6}$$

The physical amplitudes cannot depend on the way in which we split the Hilbert space and must therefore be independent of the cutoff. Consequently, $V_{\mathrm{low}\,k}$ changes or "runs" with the cutoff in order to cancel the cutoff dependence arising from the truncated intermediate state summations. This means that the effective theory must be RG invariant. Demanding RG invariance implies a RG equation

for the low momentum interaction

$$\frac{\mathrm{d}}{\mathrm{d}\Lambda}\langle f|\mathscr{A}|i\rangle = 0 \;\Rightarrow\; \frac{\mathrm{d}}{\mathrm{d}\Lambda}V_{\mathrm{low}\,k} = \beta([V_{\mathrm{low}\,k}],\Lambda)\ , \tag{7}$$

where the β function of the problem depends on the cutoff-dependent low momentum potential, as well as explicit cutoff dependence from the regularization. Starting from a bare interaction defined in the full Hilbert space, i.e., with a large cutoff, the RG equation can be solved to obtain the physically equivalent effective potential. This process is referred to as integrating out, or decimating the high-energy degrees of freedom. It can be viewed as filtering out the details of the assumed high-energy dynamics, while implicitly incorporating their detail-independent effects on the low-energy physics.

Since the virtual high-energy states propagate over distances of the order $1/\Lambda$ or shorter, the correction terms are well approximated by contact interactions, regardless of the detailed form of V_{H}. The general form of δV_{ct} should therefore be given by a sum over all local contact operators consistent with the symmetries of the problem. In the specific case of the two-body system, we have schematically (for an excellent discussion of the details of the approach, see [23]):

$$\begin{aligned}\delta V_{\mathrm{ct}}(\mathbf{r}) = {} & C_0\,\frac{1}{\Lambda^2}\,\delta^3(\mathbf{r}) + C_2\,\frac{1}{\Lambda^4}\,\nabla^2\,\delta^3(\mathbf{r}) + C_2'\,\frac{1}{\Lambda^4}\,\nabla\cdot\delta^3(\mathbf{r})\,\nabla + \cdots \\ & + C_{2n}\,\frac{1}{\Lambda^{2n+2}}\,\nabla^{2n}\,\delta^3(\mathbf{r}) + \ldots\end{aligned} \tag{8}$$

with dimensionless couplings C_{2n}. To a low-energy probe, the effective theory is indistinguishable from the underlying theory, provided the decimation has been performed exactly.

The power counting scheme of the EFT enables one to reliably truncate the correction terms, Eq. (8), and fit the couplings directly to a set of low-energy data, since a RG decimation of the underlying fundamental theory is at present not feasible. In our current approach, we will assume that the nucleon–nucleon interaction in the full Hilbert space is given by a high precision potential model, and then perform the RG decimation to low momenta exactly. In this way, the resulting low momentum potential contains all necessary counterterms to maintain exact RG invariance of the theory, and therefore reproduces the experimental phase shift data and the deuteron properties over the same kinematic range as the conventional models.

1.2. A schematic model

Before considering realistic nucleon–nucleon potential models, we apply the RG approach to a simplified schematic model that allows for a straightforward solution of the RG equation to construct $V_{\mathrm{low}\,k}$. In addition, the schematic model nicely illustrates the main point of our current approach. Independent of the schematic model constructed in the full Hilbert space, the RG decimation leads to a model-independent low momentum interaction $V_{\mathrm{low}\,k}$.

We consider a separable interaction, which we construct to approximately fit the experimental neutron–proton phase shift data in the $^1\mathrm{S}_0$ channel. For this purpose, we found the following separable

Table 1
The parameter sets of two separable models of type Eq. (10)

	I	II
n	1/2	1
α	1.8199	4.5354
g ($\mathrm{fm}^{(1-4n)/2}$)	3.1429	3.3542
m (fm^{-1})	1.0962	1.3892

interaction to be particularly useful [2]

$$V_{\mathrm{bare}}(k',k) = L(k')R(k) \tag{9}$$

$$= \frac{g}{(k'^2+m^2)^n}\left(-\frac{g}{(k^2+m^2)^n} + \frac{\alpha g(k^2+m^2)^n}{(k^2+\eta^2 m^2)^{2n}}\right) . \tag{10}$$

For the diagonal matrix elements, the analogy to the nucleon–nucleon interaction can be seen better

$$V_{\mathrm{bare}}(k,k) = -\frac{g^2}{(k^2+m^2)^{2n}} + \frac{\alpha g^2}{(k^2+\eta^2 m^2)^{2n}} . \tag{11}$$

The separable model consists of an attractive part and a short-range, $\eta > 1$, repulsive part. The strength of the repulsion, for given η, can be constructed to fit the $^1S_0$ phase shift data reasonably.

For separable potentials, the Lippmann–Schwinger equation can be resummed explicitly and one finds [22]

$$T_{\mathrm{bare}}(k',k;k^2) = \frac{L(k')R(k)}{1+(2/\pi)\mathscr{P}\displaystyle\int_0^\infty [L(p)R(p)/(p^2-k^2)]\,p^2\,\mathrm{d}\,p} . \tag{12}$$

We choose a typical $\eta = 2$, which approximately reflects the ratio of the repulsive to attractive meson contributions $m_\omega/2m_\pi$. The remaining parameters of our model, g, m and α, are then fitted to reproduce the effective range expansion,

$$T_{\mathrm{bare}}(k,k;k^2) = \frac{1}{1/a_s - \frac{1}{2}r_0 k^2} \tag{13}$$

and the change in sign of the experimental phase shifts $T_{\mathrm{bare}}(\kappa,\kappa;\kappa^2) = 0$ at $\kappa = 1.79\ \mathrm{fm}^{-1}$ for a given power n. We constructed two exemplary separable models with the parameters given in Table 1. The separable models are fitted to a neutron–proton $^1S_0$ scattering length, $a_s = -23.73$ fm, and effective range $r_0 = 2.70$ fm.

In Fig. 2, we show the phase shifts calculated from the models of V_{bare}. We observe that the separable models I and II can achieve a reasonably realistic description of the nucleon–nucleon phase shifts for laboratory energies below $E_{\mathrm{lab}} \lesssim 350$ MeV, i.e., for relative momenta $k \lesssim 2.1\ \mathrm{fm}^{-1}$.

As discussed in the previous section, the low momentum amplitudes can be preserved with an effective interaction $V_{\mathrm{low}\,k}$ acting in the Hilbert space of low momentum modes, $k < \Lambda$, exclusively.

[2] For simplicity, we have chosen different functions for $L(k')$ and $R(k)$, in order to include a repulsive part in the potential without having to introduce several separable terms, which would complicate the discussion.

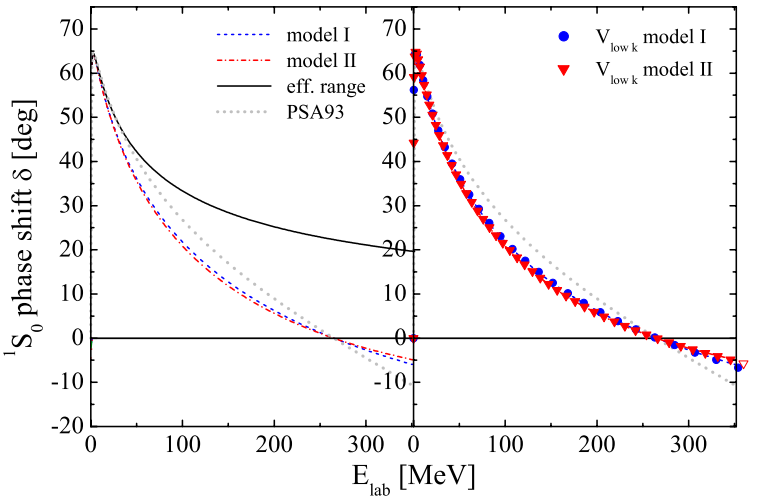

Fig. 2. The left figure shows the phase shifts calculated from the separable models I and II in comparison with the effective range expansion and the Nijmegen multi-energy phase shift analysis (PSA93) [24,25]. In the right figure, the phase shifts calculated from the corresponding low momentum interactions are given. The low momentum interactions are obtained by solving the RG equation, Eq. (14), to a scale $\Lambda = 2.1$ fm^{-1}.

The low momentum potential is renormalized by the high momentum modes according to an RG equation, of general form given by Eq. (7). In the current approach, we demand that the low momentum half-on-shell T matrix (and consequently the phase shifts) are RG invariant, see also [3,4]. The RG equation which follows from this requirement is derived in [26]. For separable interactions, the RG equation for the diagonal components of the low momentum interaction simplifies and is given in closed form by [3]

$$\frac{\mathrm{d}}{\mathrm{d}\Lambda} V_{\mathrm{low}\,k}(k,k;\Lambda) = \frac{2/\pi}{1-(k/\Lambda)^2} \frac{V_{\mathrm{low}\,k}(k,k;\Lambda)\, V_{\mathrm{low}\,k}(\Lambda,\Lambda;\Lambda)}{1+\frac{2}{\pi}\mathscr{P}\int_0^\Lambda \frac{V_{\mathrm{low}\,k}(p,p;\Lambda)}{p^2-\Lambda^2}\, p^2\,\mathrm{d}p} \ . \tag{14}$$

The initial condition of the RG equation is given by the bare interaction,

$$V_{\mathrm{low}\,k}(k,k;\Lambda_0) = V_{\mathrm{bare}}(k,k) \ , \tag{15}$$

at an initial scale Λ_0 where the high momentum modes are negligible,

$$V_{\mathrm{bare}}(\Lambda_0,\Lambda_0) \approx 0 \ . \tag{16}$$

The RG equation is then used to evolve the bare potentials to low momenta, thus removing the model-dependent realization of the high momentum parts. We solve the separable RG equation to a cutoff $\Lambda = 2.1$ fm^{-1}, which corresponds to a laboratory energy scale up to which the realistic

[3] The RG equation is regularized by imposing a small gap between the low momentum Hilbert space, $k \leqslant \Lambda - \varepsilon$, and the cutoff Λ in the integration over intermediate momenta, $p_{\mathrm{loop}} \leqslant \Lambda$. In this way the T matrix can be calculated to chosen accuracy. In other words, the effect of this regularization on the scattering amplitude is $\mathcal{O}(\varepsilon)$.

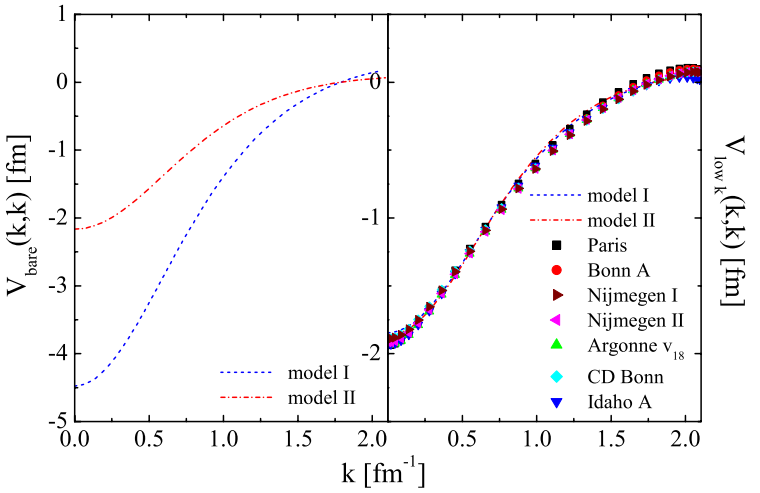

Fig. 3. The diagonal momentum-space matrix elements of $V_{\rm bare}$ and $V_{{\rm low}\,k}$ derived from the separable models I and II. As a comparison, we show the results for the diagonal matrix elements of the $V_{{\rm low}\,k}$ from Section 3 derived from the high precision nucleon–nucleon interactions.

nucleon–nucleon interactions are constrained by experiment, $E_{\rm lab} \sim 350$ MeV. First, we compare the phase shifts calculated in the low momentum space

$$\tan\delta = -kT_{{\rm low}\,k}(k,k;k^2)\ , \tag{17}$$

$$T_{{\rm low}\,k}(k,k;k^2) = \frac{V_{{\rm low}\,k}(k,k;\Lambda)}{1+(2/\pi)\,\mathscr{P}\int_0^{\Lambda}[V_{{\rm low}\,k}(p,p;\Lambda)/p^2-k^2]\,p^2\,{\rm d}p} \tag{18}$$

and verify in Fig. 2 that the phase shifts are indeed reproduced by $V_{{\rm low}\,k}$. In the RG approach, we have by construction

$$T_{{\rm low}\,k}(k',k;k^2) = T_{\rm bare}(k',k;k^2)\ . \tag{19}$$

In Fig. 3, we show the resulting diagonal matrix elements of $V_{{\rm low}\,k}$ in comparison to the $V_{{\rm low}\,k}$ derived from the high precision nucleon–nucleon interactions. Although the bare separable models I and II differ substantially, we find that the low momentum interactions in the truncated Hilbert space are identical. Furthermore, we observe that, to a surprisingly good accuracy, these simple models can in fact reproduce the diagonal matrix elements of the low momentum interaction obtained from the realistic potential models. In the RG equation for separable models, the matrix element corresponding to zero phase shift remains invariant,

$$V_{{\rm low}\,k}(\kappa,\kappa;\Lambda) = V_{\rm bare}(\kappa,\kappa) = T(\kappa,\kappa;\kappa^2) = 0\ . \tag{20}$$

Interestingly, we find that the diagonal matrix element of the realistic $V_{{\rm low}\,k}$ also changes sign approximately at relative momentum κ.

1.3. Organization

This work is organized as follows. In the next section we discuss the calculational methods used for constructing the effective low momentum interaction $V_{\mathrm{low}\,k}$. In particular, we show how $V_{\mathrm{low}\,k}$ is related to the solution of the Bloch–Horowitz equation. Since the equivalence of the model space effective interaction methods and the RG approach is discussed in detail in [26], we will focus on the discussion of the effective interaction methods used in this work. In Section 3, we present the results for the low momentum interactions derived from the realistic potential models. We give results for all partial waves with $J \leqslant 4$, which provides ample evidence for the claimed model independence of $V_{\mathrm{low}\,k}$. By studying specific partial waves, we will show how the model independence is reached as the cutoff is varied, and also demonstrate its relation to the phase shift equivalence and the common long-range pion physics of the different potential models. Finally, we verify that the low momentum interaction indeed reproduces the scattering data below $E_{\mathrm{lab}} \lesssim 350$ MeV and the deuteron binding energy with similar accuracy as the high precision potentials. After summarizing our results, we elaborate on the advantages of using $V_{\mathrm{low}\,k}$ as the microscopic input interaction for nuclear many-body calculations.

2. Calculational methods

The schematic model provides a nice example illustrating the use of nonperturbative RG techniques to construct the low momentum effective theory. One could therefore apply the same direct method as for the schematic model. However, in the general non-separable case, the direct solution of the RG equation would be more involved. Therefore, we have adapted conventional effective interaction techniques, also referred to as model space methods, for the calculation of the low momentum interaction in the general case. These methods have been successfully used to derive nuclear shell model interactions in a truncated Hilbert space, see e.g., the review [27]. Both the RG and model space techniques are concerned with integrating out the high-energy states, such that the low-energy observables remain invariant in the simpler effective theory. In spite of their similarities, the formal equivalence of conventional effective interaction theory and the RG was only recently demonstrated for the two-body problem [26]. There, we have shown that the low momentum Hamiltonian obtained from the solution of the RG equation is equivalent to the effective theory derived using Bloch–Horowitz or Lee–Suzuki projection methods. Since our current work makes use of this equivalence for the calculation of $V_{\mathrm{low}\,k}$, we briefly discuss the relevant techniques below.

2.1. Integrating out the high momentum modes by similarity transformations

Consider a physical system, for which we are only interested in its low-energy properties. The first step in effective interaction theory is to define Feshbach projection operators onto the physically important low-energy model space, the so-called P-space, and the high-energy complement, the Q-space,

$$P = \sum_{i=1}^{d} |i\rangle\langle i| = \begin{pmatrix} 1 & 0 \\ 0 & 0 \end{pmatrix} \quad \text{and} \quad Q = \sum_{i=d+1}^{\infty} |i\rangle\langle i| = \begin{pmatrix} 0 & 0 \\ 0 & 1 \end{pmatrix} . \tag{21}$$

The projection operators satisfy $P+Q=1$, $PQ=QP=0$, $P^2=P$ and $Q^2=Q$, and we have written the projection operators in matrix form as well. In most applications, the eigenstates of the unperturbed Hamiltonian H_0 are taken as basis states $|i\rangle$.

The Schrödinger equation can then be written in block form as

$$\begin{pmatrix} PHP & PHQ \\ QHP & QHQ \end{pmatrix} \begin{pmatrix} P|\Psi\rangle \\ Q|\Psi\rangle \end{pmatrix} = E \begin{pmatrix} P|\Psi\rangle \\ Q|\Psi\rangle \end{pmatrix} . \tag{22}$$

By using the second block row of Eq. (22), the Q-space projection $Q|\Psi\rangle$ can be eliminated and one obtains the fundamental equations of Bloch–Horowitz effective interaction theory [28,29]

$$P\mathscr{H}^{\mathrm{BH}}_{\mathrm{low}\,k}(E)P|\Psi\rangle = EP|\Psi\rangle , \tag{23}$$

where the effective Hamiltonian $\mathscr{H}^{\mathrm{BH}}_{\mathrm{low}\,k}(E)$ is obtained by the solution of the Bloch–Horowitz equation

$$\mathscr{H}^{\mathrm{BH}}_{\mathrm{low}\,k}(E) = H + H\,\frac{1}{E-QHQ}\,H . \tag{24}$$

The Bloch–Horowitz equation generates an effective Hamiltonian, whose P-space projection $H^{\mathrm{BH}}_{\mathrm{low}\,k}(E)=P\,\mathscr{H}^{\mathrm{BH}}_{\mathrm{low}\,k}(E)\,P$ is operative only within the low-energy model space and, e.g., enables an exact diagonalization in shell model applications. The Q-space states have been decoupled from the problem in a way that preserves the low-energy spectrum exactly, i.e., the d lowest-lying eigenvalues. The eigenstates of $H^{\mathrm{BH}}_{\mathrm{low}\,k}(E)$ are simply given by the P-space projections of the exact eigenstates $P|\Psi_n\rangle$. The effective Hamiltonian $H^{\mathrm{BH}}_{\mathrm{low}\,k}(E)$ depends on the exact energy eigenvalue one is solving for, and thus necessitates a self-consistent treatment. Although the self-consistency problem can be solved nicely using the Lanczos algorithm [30], the use of energy-dependent two-body interactions in many-body calculations can pose computational and conceptual difficulties.

A refinement of the Bloch–Horowitz theory that avoids these difficulties is the Lee–Suzuki similarity transformation [31,32]. The Lee–Suzuki method constructs a similarity transformation that brings the Hamiltonian to the following block structure:

$$\Theta^{-1}\,H\,\Theta = \mathscr{H}^{\mathrm{LS}}_{\mathrm{low}\,k} = \begin{pmatrix} P\,\mathscr{H}\,P & P\,\mathscr{H}\,Q \\ 0 & Q\,\mathscr{H}\,Q \end{pmatrix} . \tag{25}$$

Since the determinant of a block-triangular matrix factorizes into the determinants of the independent P- and Q-space blocks, the low-energy spectrum can be calculated exactly from the smaller effective model space Hamiltonian $H^{\mathrm{LS}}_{\mathrm{low}\,k} = P\,\mathscr{H}^{\mathrm{LS}}_{\mathrm{low}\,k}\,P$. As in the Bloch–Horowitz approach, the eigenstates of $H^{\mathrm{LS}}_{\mathrm{low}\,k}$ are given by $P|\Psi_n\rangle$. Making an ansatz for the Lee–Suzuki similarity transformation, one parametrizes Θ as a non-orthogonal transformation in terms of the so-called wave operator ω

$$\Theta = 1+\omega = \begin{pmatrix} 1 & 0 \\ \omega & 1 \end{pmatrix} \quad \text{and} \quad \Theta^{-1} = 1-\omega = \begin{pmatrix} 1 & 0 \\ -\omega & 1 \end{pmatrix} , \tag{26}$$

where $\omega = Q\,\omega\,P$ connects the Q- and P-space. Inserting the ansatz into Eq. (25) leads to a non-linear constraint on ω, the decoupling equation,

$$Q\,\mathscr{H}^{\mathrm{LS}}_{\mathrm{low}\,k}\,P = 0 \;\Rightarrow\; QHP + QHQ\,\omega - \omega\,PHP - \omega\,PHQ\,\omega = 0 . \tag{27}$$

Once a solution to this non-linear operator equation is found, the energy-independent effective Hamiltonian is given by

$$H^{\mathrm{LS}}_{\mathrm{low}\,k} = PHP + PHQ\,\omega\,P = PHP + PVQ\,\omega\,P\ , \tag{28}$$

where we have assumed that P and Q commute with the unperturbed Hamiltonian.

The relation to the Bloch–Horowitz theory can be clarified by inserting the Lee–Suzuki solution, Eq. (28), into the decoupling equation, Eq. (27), and solving for the wave operator. The resulting formal expression for the wave operator allows one to express the energy-independent Lee–Suzuki $H^{\mathrm{LS}}_{\mathrm{low}\,k}$ as a summation of the lowest d, self-consistent Bloch–Horowitz solutions $H^{\mathrm{BH}}_{\mathrm{low}\,k}(E)$, where each term is weighted by the projection of the corresponding eigenstate of the effective theory $P\,|\Psi_n\rangle(\langle\widetilde{\Psi_n}|\,P)$[4]

$$\begin{aligned} H^{\mathrm{LS}}_{\mathrm{low}\,k} &= \sum_{n=1}^{d}\left(PHP + PH\,\frac{1}{E_n - QHQ}\,HP\right)P\,|\Psi_n\rangle(\langle\widetilde{\Psi_n}|\,P) \\ &= \sum_{n=1}^{d} H^{\mathrm{BH}}_{\mathrm{low}\,k}(E_n)\,P\,|\Psi_n\rangle(\langle\widetilde{\Psi_n}|\,P)\ . \end{aligned} \tag{29}$$

In this work, we apply the Lee–Suzuki formalism to the free-space nucleon–nucleon problem to derive the energy-independent low momentum interaction

$$V_{\mathrm{low}\,k} = H^{\mathrm{LS}}_{\mathrm{low}\,k} - PH_0P = PVP + PVQ\,\omega\,P\ . \tag{30}$$

This approach has been proven to be equivalent to the solution of the RG equation that results from imposing a momentum-space cutoff and demanding RG invariant half-on-shell (HOS) T matrices [26]. For a given partial wave, the P and Q operators are defined in a continuous plane wave basis as

$$P = \frac{2}{\pi}\int_0^{\Lambda} p^2\,\mathrm{d}p\,|p\rangle\langle p| \quad \text{and} \quad Q = \frac{2}{\pi}\int_{\Lambda}^{\infty} q^2\,\mathrm{d}q\,|q\rangle\langle q|\ . \tag{31}$$

There are several methods to solve the non-linear decoupling equation for the wave operator. For the two-body problem, e.g., the exact solutions for the eigenstates can be used, and $V_{\mathrm{low}\,k}$ can be calculated directly using Eq. (29). For more complex applications, one solves the decoupling equation using iterative techniques. Since the iterative methods are numerically very robust, we have utilized the iterative algorithm of Andreozzi [33] to calculate $V_{\mathrm{low}\,k}$. The defining equations of this iteration scheme are given by

$$\mathcal{X}_0 = -(QHQ)^{-1}\,QHP\ , \tag{32}$$

$$\mathcal{X}_n = (\mathcal{Q}(\omega_{n-1}))^{-1}\,\mathcal{X}_{n-1}\,H^{\mathrm{LS}}_{\mathrm{low}\,k}(\omega_{n-1}) \quad \text{for } n \geqslant 1\ , \tag{33}$$

where

$$\omega_n = \mathcal{X}_0 + \mathcal{X}_1 + \cdots + \mathcal{X}_n\ , \tag{34}$$

$$\mathcal{Q}(\omega_n) = QHQ - Q\,\omega_n\,PHQ \tag{35}$$

[4] The tilde denotes the bi-orthogonal complement, since projections of orthogonal $|\Psi_n\rangle$ are not necessarily orthogonal.

and

$$H^{\rm LS}_{{\rm low}\,k}(\omega_n) = PHP + PHQ\,\omega_n\,P\ . \tag{36}$$

The iteration converges when $H^{\rm LS}_{{\rm low}\,k}(\omega_n) \approx H^{\rm LS}_{{\rm low}\,k}(\omega_{n-1})$.

A convenient feature of the algorithm is that each iteration only requires one matrix inversion in the Q-space. The Q-space matrix inversion is manageable, typically requiring a set of ≈ 60 Gauss–Legendre mesh points extending to ≈ 25 fm^{-1} to include the high momentum behavior of the input interaction. Finally, we mention that variations of the algorithm exist in which all matrix inversions occur in P-space, which can offer significant computational advantages for large-scale problems [33].

2.2. A refinement: hermitian low momentum interactions

By construction, the Lee–Suzuki $H^{\rm LS}_{{\rm low}\,k}$ is non-hermitian because the eigenstates of the effective theory are projections of the full eigenstates onto the low momentum subspace. The non-hermiticity is a result of eliminating the energy-dependence of the Bloch–Horowitz theory by means of the non-orthogonal similarity transformation.[5] However, one can perform an additional similarity transformation on $H^{\rm LS}_{{\rm low}\,k}$ to obtain an energy-independent and hermitian Hamiltonian [34,35], which we denote by $\bar{H}^{\rm LS}_{{\rm low}\,k}$ and correspondingly, the hermitian low momentum interaction by $\bar{V}_{{\rm low}\,k}$. Both similarity transformations combine to give a unitary transformation, which is equivalent to the well-known Okubo transformation [36].

Here, we follow the method of Andreozzi [33] in constructing the second similarity transformation. Using the definition of the Lee–Suzuki transformation, Eq. (25), one finds

$$\Theta^\dagger\Theta\,\mathscr{H}^{\rm LS}_{{\rm low}\,k} = (\mathscr{H}^{\rm LS}_{{\rm low}\,k})^\dagger\,\Theta^\dagger\Theta\ , \tag{37}$$

where we have used $H = H^\dagger$. Projecting onto the low momentum space, the P-space block can be written as

$$(P + \omega^\dagger\,\omega)\,H^{\rm LS}_{{\rm low}\,k} = (H^{\rm LS}_{{\rm low}\,k})^\dagger\,(P + \omega^\dagger\omega)\ . \tag{38}$$

The operator $P + \omega^\dagger\,\omega$ is hermitian and positive definite. Therefore, it can be written by means of a Cholesky decomposition as a product of a lower-triangular matrix L and its adjoint $L^\dagger$. Writing

$$(P + \omega^\dagger\,\omega) = LL^\dagger \tag{39}$$

in Eq. (38) and multiplication by L^{-1} from the left and $(L^\dagger)^{-1}$ from the right, one finds

$$L^{-1}\,(\mathscr{H}^{\rm LS}_{{\rm low}\,k})^\dagger\,L = L^\dagger\,\mathscr{H}^{\rm LS}_{{\rm low}\,k}\,(L^\dagger)^{-1} = (L^{-1}(\mathscr{H}^{\rm LS}_{{\rm low}\ k})^\dagger L)^\dagger\ . \tag{40}$$

Therefore, we can write the hermitian $\bar{H}^{\rm LS}_{{\rm low}\,k}$ directly in terms of the Lee–Suzuki transformation and the Cholesky decomposition as

$$\bar{H}^{\rm LS}_{{\rm low}\,k} = L^\dagger\,H^{\rm LS}_{{\rm low}k}\,(L^\dagger)^{-1} \tag{41}$$

and the combined transformation $U = \Theta\,(L^\dagger)^{-1}$ is unitary.

---

[5] Although the Bloch–Horowitz Hamiltonian $H^{\rm BH}_{{\rm low}\,k}(E_n)$ is hermitian for a given energy E_n, one encounters the same non-orthogonality problem between eigenstates, since the Hamiltonian changes self-consistently depending on the energy E_n.

We mention that the differences between the non-hermitian $V_{\mathrm{low}\,k}$ and the hermitian $\bar{V}_{\mathrm{low}\,k}$ can be understood in the RG approach. The non-hermitian effective theory is obtained by introducing a cutoff in momentum space and imposing RG invariance for the HOS T matrix with an energy-independent low momentum potential. Since the initial conditions of the RG equation are given by the bare interaction, this implies that the effective theory preserves the low momentum components of the full wave functions, in addition to the phase shifts and the bound state poles. The choice of HOS T matrix invariance is motivated by the physical observation that the low momentum components of the wave functions mainly probe the long-range OPE part of the interaction. Conversely, the hermitian effective theory results from RG invariant on-shell T matrices. Thus, the resulting hermitian $\bar{V}_{\mathrm{low}\,k}$ no longer preserves the low momentum components of the full wave functions, although the observable phase shifts and bound state poles are preserved. In practice, we will find that the numerical differences between the hermitian and non-hermitian interactions are quite small.

Finally, we note that the Lee–Suzuki similarity transformation method is an algebraic realization of the more general folded diagram method of Kuo, Lee and Ratcliff (see [27,37,38]). In this connection, one can recast the results of this section in a diagrammatic formalism, which can be useful in many-body systems. Moreover, the folded diagram formulation has been applied to the two-body problem to prove diagrammatically that the low momentum effective theory preserves the low-energy scattering observables of the input interaction [3].

3. Results

We now discuss the main results for the low momentum interaction $V_{\mathrm{low}\,k}$, which we have obtained by integrating out the high momentum components of different realistic potential models. Most of the results shown here are for a momentum cutoff of $\Lambda = 2.1\ \mathrm{fm}^{-1}$, which corresponds to a distance scale $1/\Lambda \sim 0.5$ fm. With cutoffs chosen in this range, the model-dependent parameterization of the repulsive core at $r \lesssim 0.5$ fm in the bare interactions is not resolved in the effective theory. Consequently, one is able to reproduce the deuteron pole and scattering observables below $E_{\mathrm{lab}} = 350$ MeV without introducing a specific short-distance model. Moreover, the RG invariance of the decimation guarantees that our conclusions are independent of the precise value of the cutoff.

Before we present our results in detail, we summarize our main findings and refer the reader to the key figures. The most important properties of $V_{\mathrm{low}\,k}$ are:

1. $V_{\mathrm{low}\,k}$ renormalizes to a nearly universal interaction as the cutoff is lowered to the scale of $\Lambda \sim 2.1\ \mathrm{fm}^{-1}$. We will argue that the model independence of the diagonal matrix elements of $V_{\mathrm{low}\,k}$, as shown in Figs. 4 and 5, is driven by the phase shift equivalence of the input models. The correlation between the phase shift equivalence and the collapse of the low momentum interactions is clearly demonstrated in Fig. 8. We also find practically identical results for the hermitian $\bar{V}_{\mathrm{low}\,k}$, see Figs. 18 and 19.
2. $V_{\mathrm{low}\,k}$ reproduces the phase shifts and the deuteron binding energy with similar accuracy as the high precision models. The phase shifts calculated from $V_{\mathrm{low}\,k}$ are shown in Figs. 16 and 17.
3. In the effective theory one does not have to make model-dependent assumptions on the short-distance interaction. The RG evolution filters out the short-distance details of the input potentials, while preserving the model-independent effects of the high momentum modes on the low

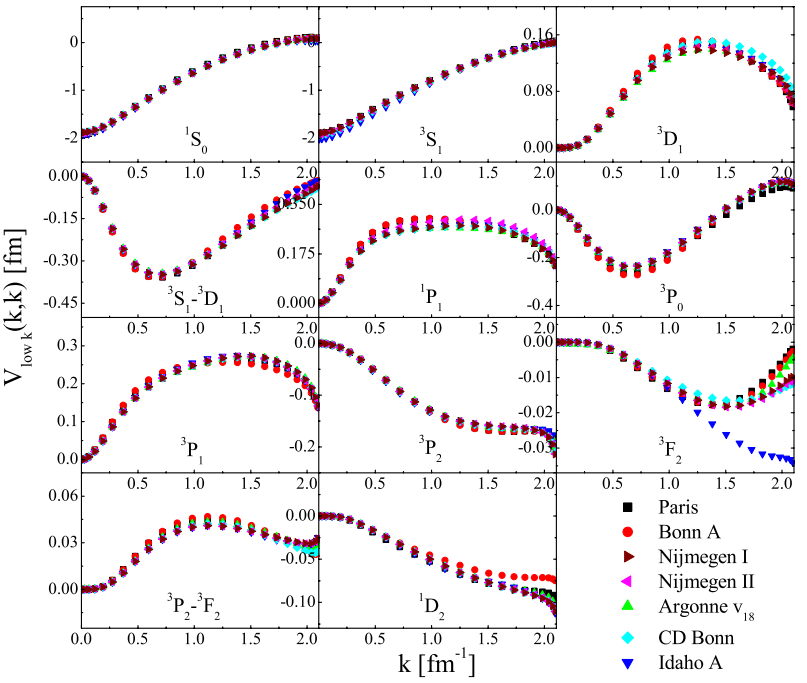

Fig. 4. Diagonal momentum-space matrix elements of the $V_{\mathrm{low}\,k}$ obtained from the different potential models for a cutoff $\Lambda = 2.1$ fm^{-1}. Results are shown for the partial waves $J \leqslant 4$.

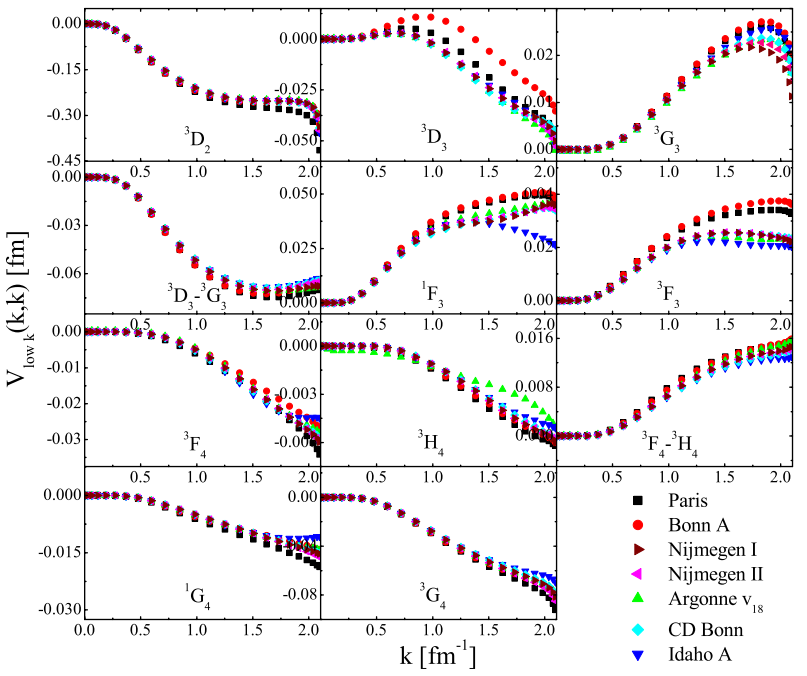

Fig. 5. The diagonal matrix elements of $V_{\mathrm{low}\,k}$ are continued from Fig. 4.

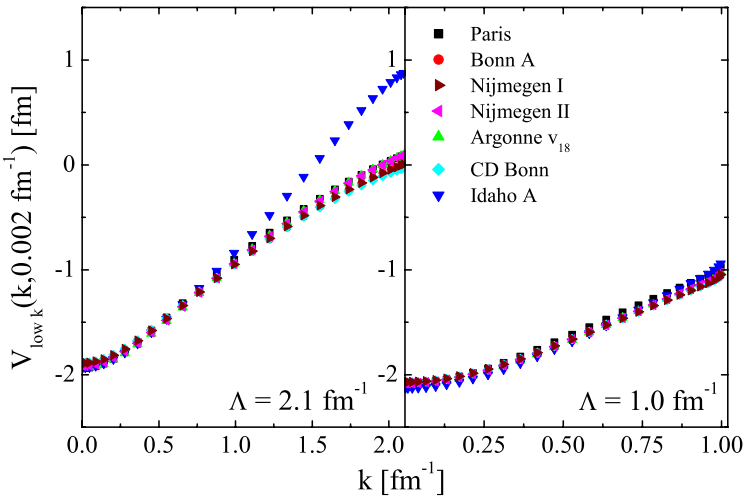

Fig. 6. The off-diagonal momentum space matrix elements of the $V_{\mathrm{low}\,k}$ obtained for a cutoff $\Lambda = 2.1$ fm^{-1} (left) and $\Lambda = 1.0$ fm^{-1} (right) in the $^1S_0$ partial wave.

momentum observables, and leaving the long-range part (OPE) of the interaction intact. This can be seen most clearly in Figs. 11–13.

We also point out that the numerical differences between $V_{\mathrm{low}\,k}$ and the hermitian $\bar{V}_{\mathrm{low}\,k}$ are quite small, see Fig. 15. For brevity, we mostly present results for $V_{\mathrm{low}\,k}$ in this work, since the $\bar{V}_{\mathrm{low}\,k}$ is easily derived from $V_{\mathrm{low}\,k}$ using the transformation described in Section 2.2.

3.1. Model independence of the low momentum interaction

For cutoffs around $\Lambda \sim 2.1$ fm^{-1}, the effective theory preserves the nucleon–nucleon phase shifts up to laboratory energies of $E_{\mathrm{lab}} \sim 350$ MeV. This corresponds to the scale of the scattering data that all the high precision potential models are fitted to. We have argued that, based on the separation of mass scales, the model dependence of the realistic interactions should be reduced as we integerate out the ambiguous high momentum modes. In Figs. 4 and 5, we present the results of the RG decimation. We observe that the diagonal matrix elements of the low momentum interactions derived from the different potential models are nearly identical, and thus insensitive to the input potential model for cutoffs $\Lambda \lesssim 2.1$ fm^{-1}. The largest relative differences between the $V_{\mathrm{low}\,k}$ are found in the $^3F_2$, $^3D_3$, $^1F_3$ and $^3F_3$ partial waves. These differences are correlated with the deviations in the phase shifts, i.e., the different accuracies, of the potential models. We will discuss this point in detail below.

We note that if we perform the additional similarity transformation to obtain the resulting hermitian $\bar{V}_{\mathrm{low}\,k}$, we find the same model independence and practically identical diagonal matrix elements, as shown in Figs. 18 and 19 in the appendix. Since the hermitian $\bar{V}_{\mathrm{low}\,k}$ is obtained by symmetrizing $V_{\mathrm{low}\,k}$, it is expected that the effects on the diagonal matrix elements are not significant.

One obtains further insight into the collapse of $V_{\mathrm{low}\,k}$ by studying the off-diagonal matrix elements. These are shown in the $^1S_0$ partial wave in Fig. 6. We find a similar nearly universal behavior for the off-diagonal matrix elements of $V_{\mathrm{low}\,k}$, although those calculated from the Idaho potential differ at $k' \approx 1.2$ fm^{-1}, which is approximately the mass scale given by the 2π exchange. The conventional

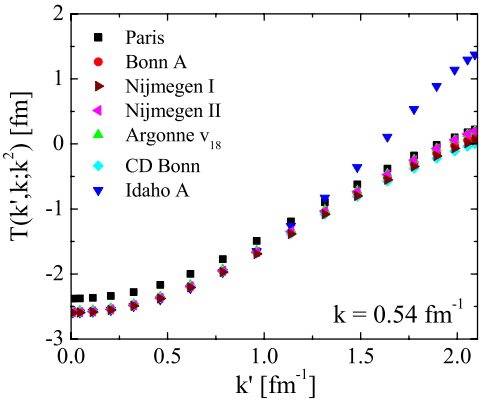

Fig. 7. Comparison of the HOS T matrices calculated from the different potential models in the $^1S_0$ partial wave.

models include 2π contributions in which non-nucleonic intermediate states are explicitly taken into account. In contrast, the Idaho potential starts from a local, effective Lagrangian, in which nucleons and pions are the only explicit degrees of freedom. For example, contributions from Δ intermediate states between two successive pion exchanges are contracted to a renormalized $\mathscr{L}^{\text{eff}}_{\pi\text{NN}}$ vertex. Moreover, the conventional potential models all contain a strong, short-range repulsion associated with the exchange of heavy mesons, mostly originating from the ω exchange. In the Idaho potential, the repulsive core is not explicitly present. However, the effects of the short-range repulsion on low-energy observables are contained in contact terms that are fitted to the low-energy data [19]. Therefore, in momentum space, the Idaho potential changes over to contact terms at momentum transfers above the range given by $2m_\pi$.

While the Idaho potential is phase shift equivalent to the conventional models, the HOS T matrices, i.e., the low momentum components of the wave functions, differ significantly from the conventional models at energies and momenta larger than the above scale of $2m_\pi$. In Fig. 7, we find that the conventional models give remarkably similar HOS T matrices over their range of phase shift equivalence. This approximate HOS T matrix equivalence can be understood by expanding the HOS T matrix around the fully on-shell part. The difference can be written as a wound integral that contains the off-shell behavior,

$$T(k',k;k^2) = T(k,k;k^2) + \frac{k^2 - k'^2}{k'} \int_0^\infty \mathrm{d}r \sin(k'r)(u_k(r) - v_k(r)) \ , \tag{42}$$

where $u_k(r) = r\,\Psi_k(r)$ denotes the exact and $v_k(r)$ is the asymptotic S-wave wave function

$$\lim_{r\to\infty} u_k(r) \to v_k(r) \sim \sin(kr + \delta) \ . \tag{43}$$

We can use Eq. (42) to express the difference of the HOS T matrices for two different, but phase shift equivalent bare interactions. This leads to

$$\Delta T(k',k;k^2) = \frac{k^2 - k'^2}{k'} \int_0^R \mathrm{d}r \sin(k'r)\Delta u_k(r) \ , \tag{44}$$

where R is the distance over which the two models differ substantially at short distances, which we can take for simplicity as the size of the repulsive core. Regardless of the details of the differences, at

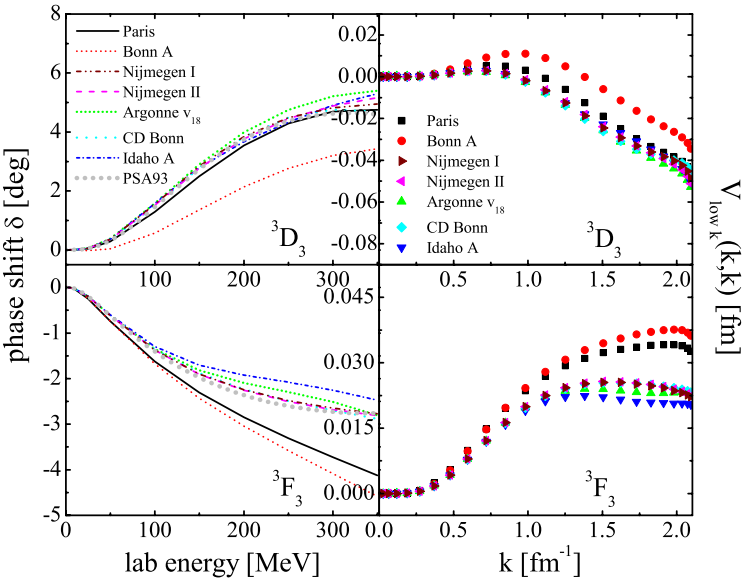

Fig. 8. Comparison of the phase shifts given by the $V_{\rm NN}$ models and the diagonal matrix elements of $V_{\rm low\,k}$ in the $^3D_3$ and $^3F_3$ partial waves. Results for $V_{\rm low\,k}$ are shown with a cutoff $\Lambda = 2.1$ fm^{-1}.

scattering energies well below the strength of the short-range repulsion, the differences between the wave functions in the core are suppressed by strong two-body correlations. Therefore, it is physically reasonable that the conventional realistic potentials give similar HOS T matrices at low energies.

The deviations in the off-diagonal matrix elements of $V_{\rm low\,k}$ derived from the Idaho potential are obviously removed, if we integrate out further below $2m_\pi$. As shown in Fig. 6, we find that the off-diagonal matrix elements in the $^1S_0$ partial wave collapse onto one curve as well for $\Lambda \lesssim 1.2$ fm^{-1}.

The preceding observations strongly suggest that the collapse of the diagonal matrix elements of $V_{\rm low\,k}$ is driven by the phase shift equivalence of the input models, while the collapse of the off-diagonal matrix elements is controlled by approximate HOS T matrix equivalence at low energy and momentum. The latter can in turn be mainly attributed to a common off-shell behavior in the OPE interaction, with some differences arising from the two-pion exchange and the crossover to contact interactions. The correlation between the diagonal matrix elements and the phase shifts is nicely shown in the $^3D_3$ and $^3F_3$ partial waves, where we observe the largest relative deviations from model independence. The left panels of Fig. 8 clearly show that the older generation Paris and Bonn potential models give significantly different phase shifts in these partial waves. This leads to the observed differences in the $V_{\rm low\,k}$ derived from these bare interactions, as can be seen in the right panels of Fig. 8. For comparison, we have also shown the results of the Nijmegen multi-energy phase shift analysis (PSA93) [24,25].

A further example of this correlation can be seen in Fig. 9, where the Idaho potential leads to considerably different phase shifts in the $^3F_2$ partial wave above laboratory energies $E_{\rm lab} \gtrsim 100$ MeV. This corresponds to a relative momentum of $k \gtrsim 1.0$ fm^{-1}. Accordingly in Fig. 10, we find that the diagonal matrix elements of $V_{\rm low\,k}$ derived from the Iadaho potential deviate from the others

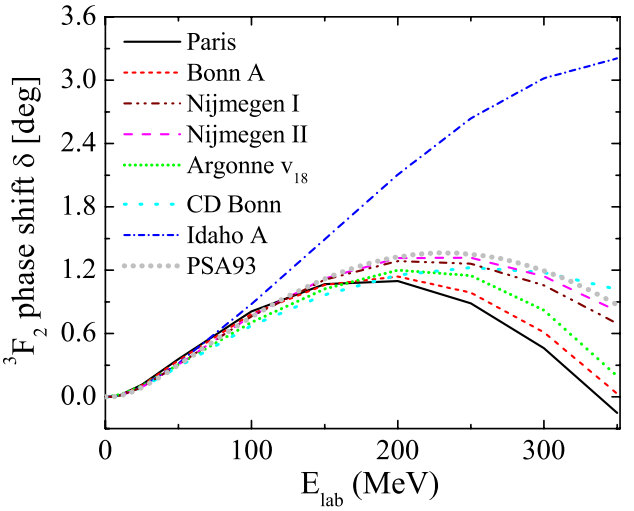

Fig. 9. Phase shifts in the $^3F_2$ partial wave calculated from different V_{NN} models.

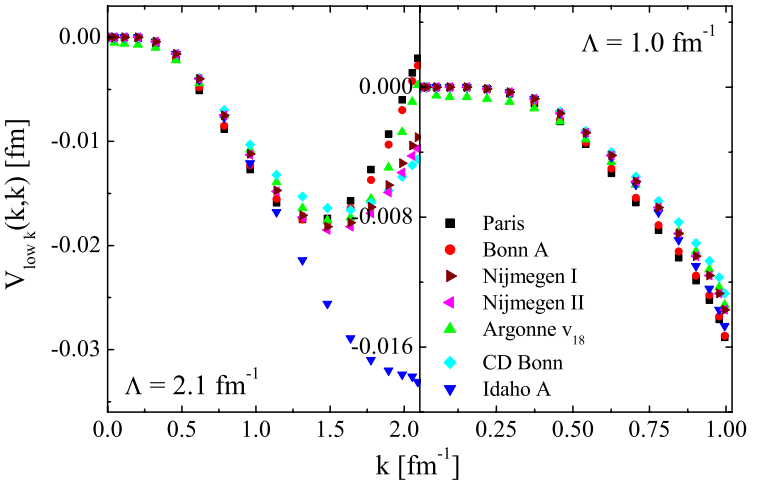

Fig. 10. The diagonal matrix elements of $V_{\mathrm{low}\,k}$ for $\Lambda = 2.1$ fm^{-1} (left) and $\Lambda = 1.0$ fm^{-1} (right) in the $^3F_2$ partial wave.

for momenta larger than this scale. As for the off-diagonal matrix elements in the $^1S_0$ partial wave, these differences vanish as the cutoff is lowered to $\Lambda \lesssim 1.0$ fm^{-1}.

In the N^{2}LO version of the Idaho potential used here, the contact interactions do not contribute to the $L \geqslant 3$ partial waves. Thus, in the $^3F_2$ partial wave the Idaho potential is completely given by pion exchange. Our results demonstrate that the effects of the short-distance physics cannot simply be ignored. Rather, their renormalization effects on the low momentum physics has to be taken into account. If we lower the cutoff to $\Lambda \lesssim 1.0$ fm^{-1}, the effects of the high momentum modes is sufficiently small, and one finds that indeed the physics is given adequately

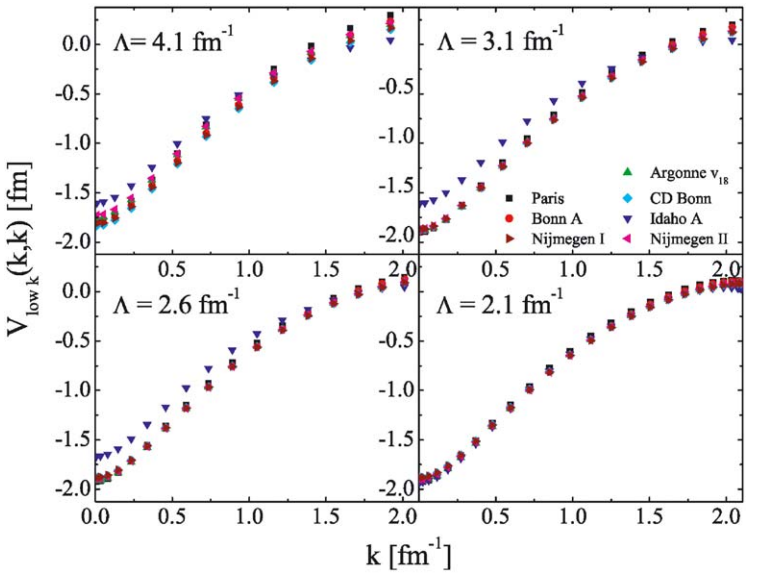

Fig. 11. The collapse of the diagonal momentum-space matrix elements of $V_{\mathrm{low}\,k}$ as the cutoff is lowered to $\Lambda = 2.1$ fm^{-1} in the $^1S_0$ partial wave.

by pion exchange. This can be understood in the Born approximation, which is a reasonable approximation for the high partial waves, especially at low energies. In the Born approximation, the integral term of the Lippmann–Schwinger equation is neglected, and thus the low momentum interaction in the cutoff Hilbert space is given by simply cutting off the bare interaction.

The RG approach has the advantage that the nature of the low momentum interaction can be revealed by studying the change of $V_{\mathrm{low}\,k}$ with the cutoff scale. In this way, the RG evolution clearly provides evidence for the separation of scales in the two-nucleon problem, see also [3]. Furthermore, we will show that it also provides physical insight into the low momentum interaction.

In the evolution of the $^1S_0$ matrix elements shown in Fig. 11, we find that the model independence of $V_{\mathrm{low}\,k}$ is reached at somewhat larger values of the cutoff around $\Lambda \sim 3.5$ fm^{-1}. This scale lies below the ω and ρ meson masses, and consequently the details of the repulsive core are not resolved in the effective theory. Also note that for $\Lambda \gtrsim 3.0$ fm^{-1}, the Idaho potential is not renormalized, since it is an EFT potential without high momentum components by construction.

Conversely, we find in Fig. 12 that the collapse in the $^3S_1$ partial wave occurs at a comparatively lower value for the cutoff of $\Lambda \sim 2.1$–2.6 fm^{-1}. This arises from the fact that the tensor force is operative in the triplet S-wave. Since $V_{\mathrm{low}\,k}$ acquires a large second-order renormalization from the tensor force, one indeed expects that $V_{\mathrm{low}\,k}$ becomes model-independent at a lower cutoff in the $^3S_1$ partial wave.

The nature of the tensor interaction of $V_{\mathrm{low}\,k}$ can be studied by considering the couping between the $^3S_1$ and $^3D_1$ partial wave. In this channel, only the tensor force enters. The results for the RG evolution in the $^3S_1$–$^3D_1$ block are presented in Fig. 13. We observe that the realistic models are practically identical for momenta below $k \lesssim 0.7$ fm^{-1}, which corresponds to the pion mass. This clearly demonstrates that the tensor part of the input models differs significantly for momenta above

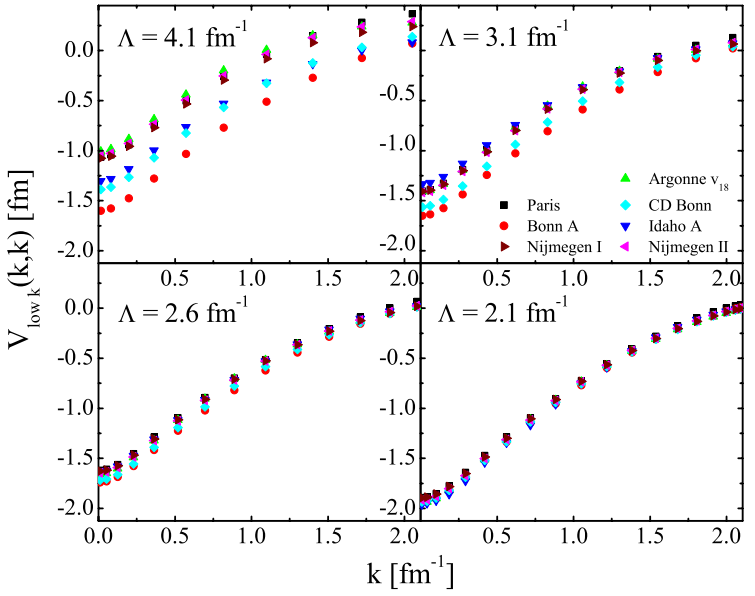

Fig. 12. The collapse of the diagonal momentum-space matrix elements of $V_{\text{low}\,k}$ as the cutoff is lowered to $\Lambda = 2.1$ fm^{-1} in the $^3S_1$ partial wave.

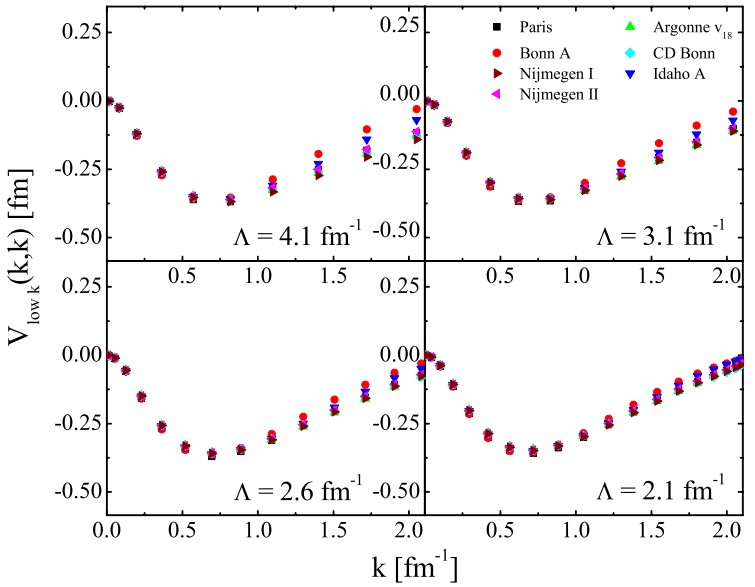

Fig. 13. The collapse of the diagonal momentum-space matrix elements of $V_{\text{low}\,k}$ as the cutoff is lowered to $\Lambda = 2.1$ fm^{-1} in the coupled $^3S_1$–$^3D_1$ block.

m_π. However, the effects of the different high momentum tensor components on the low momentum physics can be taken into account by employing a renormalized interaction, which in turn becomes model independent at a cutoff of $\Lambda \sim 2.1$ fm^{-1}.

Table 2
Comparison of the deuteron binding energy E_D for $V_{low\,k}$ and the bare interactions. We note that all $V_{low\,k}$ are derived with the same momentum mesh. For the values reported here, we have chosen not to optimize the mesh for each bare interaction separately

E_D (MeV)	Paris	Bonn A	Nijm. I	Nijm. II	Arg. v_{18}	CD Bonn	Idaho A
V_{NN}	−2.2218	−2.2242	−2.2246	−2.2242	−2.2247	−2.2238	−2.2242
Quoted	−2.2249	−2.22452	−2.224575	−2.224575	−2.224575	−2.224575	−2.2242
$V_{low\,k}$	−2.2218	−2.2242	−2.2246	−2.2242	−2.2247	−2.2238	−2.2242

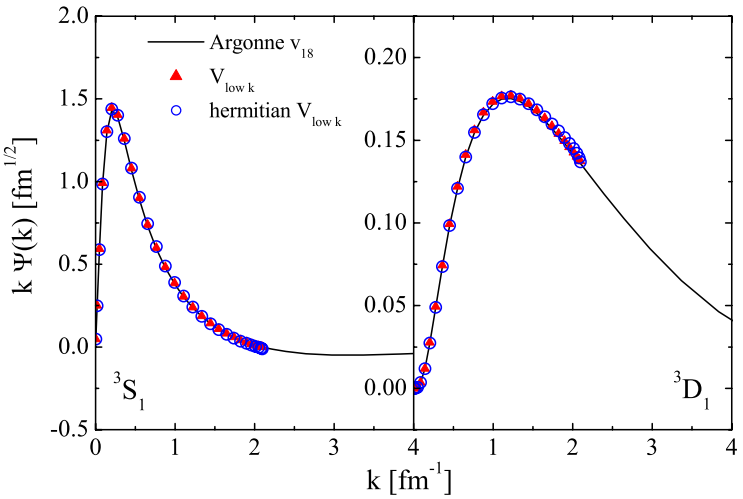

Fig. 14. Comparison of the momentum-space S- and D-state deuteron wave functions calculated from $V_{low\,k}$, the hermitian $\bar{V}_{low\,k}$ and the bare V_{NN}. Results are shown for a cutoff of $\Lambda = 2.1$ fm^{-1} and the Argonne v_{18} potential.

The RG decimation to $V_{low\,k}$ preserves the deuteron binding energies of the bare interactions. In Table 2, we give the binding energies obtained from the $V_{low\,k}$, and verify that the deuteron poles are in fact reproduced in the effective theory. We note that we have not optimized the momentum mesh for each input V_{NN}, which would further improve the agreement with the quoted values. Referring to Fig. 14, the low momentum components of the bare deuteron S- and D-state wave functions are RG invariant as well. Moreover, although the hermitian $\bar{V}_{low\,k}$ does not exactly preserve the low momentum projections of the wave functions, we find in Fig. 14 that the deuteron wave functions calculated from $V_{low\,k}$ and the hermitian $\bar{V}_{low\,k}$ are practically identical.

Finally, we note that the same general results hold for both $V_{low\,k}$ and $\bar{V}_{low\,k}$, and that the numerical differences are quite small. This is demonstrated as an example for the $^1S_0$ partial wave in Fig. 15. It can also be seen that the differences are as expected most noticeable for the far off-shell parts of the low momentum interaction.

3.2. Phase shift equivalence of the low momentum interaction

The model-independent low momentum interaction reproduces the experimental phase shift data with similar accuracy as the high precision nucleon–nucleon potentials. Therefore, $V_{low\,k}$ fits the

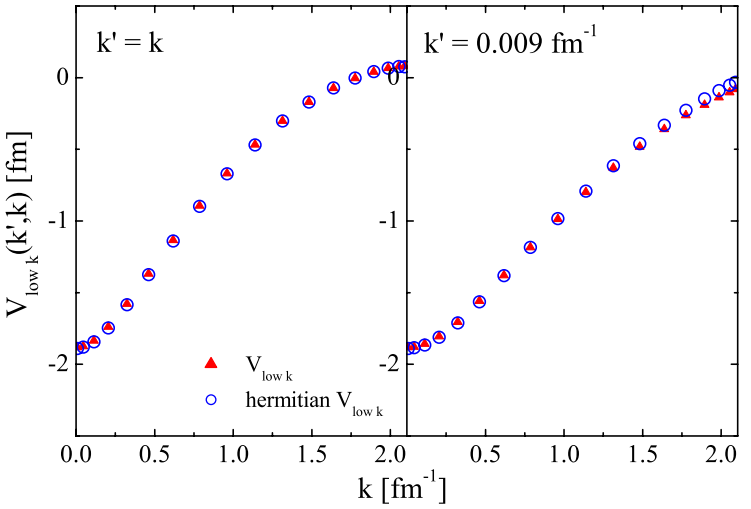

Fig. 15. Comparison of the diagonal (left) and off-diagonal (right) matrix elements of $V_{\mathrm{low}\,k}$ and the hermitian $\bar{V}_{\mathrm{low}\,k}$ in the $^1S_0$ partial wave. Results are shown for a cutoff of $\Lambda = 2.1$ fm^{-1} and the Argonne v_{18} potential.

measured phase shifts for laboratory energies below $E_{\mathrm{lab}} = 350$ MeV with a similar χ^2/datum $\approx$ 1–2, depending on which conventional potential model V_{NN} is used. Since the hermitian $\bar{V}_{\mathrm{low}\,k}$ preserves this content as well as the hermiticity of the Hamiltonian, we demonstrate the high accuracy of the hermitian $\bar{V}_{\mathrm{low}\,k}$ here. In Figs. 16 and 17, the neutron–proton phase shifts and the mixing parameters in coupled channels for all partial waves $J \leqslant 4$ are given. For clarity of the figures, we show these for the low momentum $\bar{V}_{\mathrm{low}\,k}$ derived from the CD Bonn potential only. Since both the hermitian and non-hermitian low momentum interactions preserve the phase shifts of the input models, results of the same accuracy are derived from the various other models. For comparison, the phase shifts and mixing parameters calculated from the bare CD Bonn potential and the results of the Nijmegen multi-energy phase shift analysis [24,25] are included in Figs. 16 and 17.

We conclude that the low-energy scattering data can be equally well reproduced by an effective low momentum interaction $V_{\mathrm{low}\,k}$ restricted to the Hilbert space of low momentum modes, $k < \Lambda_{\mathrm{data}}$. This is achieved with a model-independent interaction, without introducing further assumptions on the details of the short-distance dynamics.

4. Summary and advantages

We have shown that the RG decimation of different high precision nucleon–nucleon interactions to low momenta leads to a unique interaction, called $V_{\mathrm{low}\,k}$. This result is obtained by truncating the full Hilbert space to an effective space, which consists of momentum components up to the scale of the constraining low-energy data. The differences in the realistic interactions arise from the assumed high momentum dynamics. By restricting the interaction to the low momentum space, the details of the short-distance physics are not resolved, and the detail-independent effects of the high momentum modes on the low momentum observables are included in the renormalized effective interaction. The existence of a nearly universal $V_{\mathrm{low}\,k}$ demonstrates that it is possible to separate the physics of

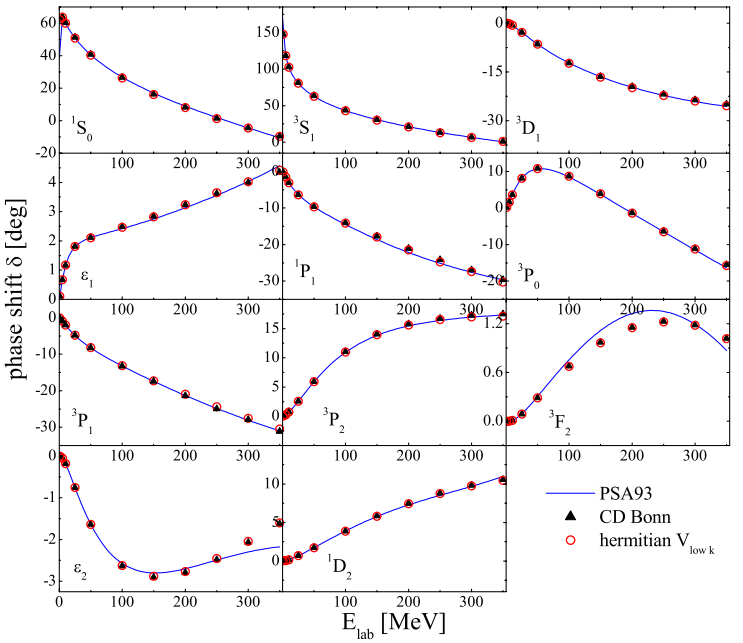

Fig. 16. The neutron–proton phase shifts and mixing parameters calculated from the hermitian $\bar{V}_{\mathrm{low}\,k}$ in the partial waves $J \leqslant 4$ are shown. The $\bar{V}_{\mathrm{low}\,k}$ is derived from the CD Bonn potential with a cutoff of $\Lambda = 2.1$ fm^{-1}. In comparison, the phase shifts and mixing parameters calculated from the bare CD Bonn potential as well as the results of the Nijmegen multi-energy phase shift analysis [24,25] are included.

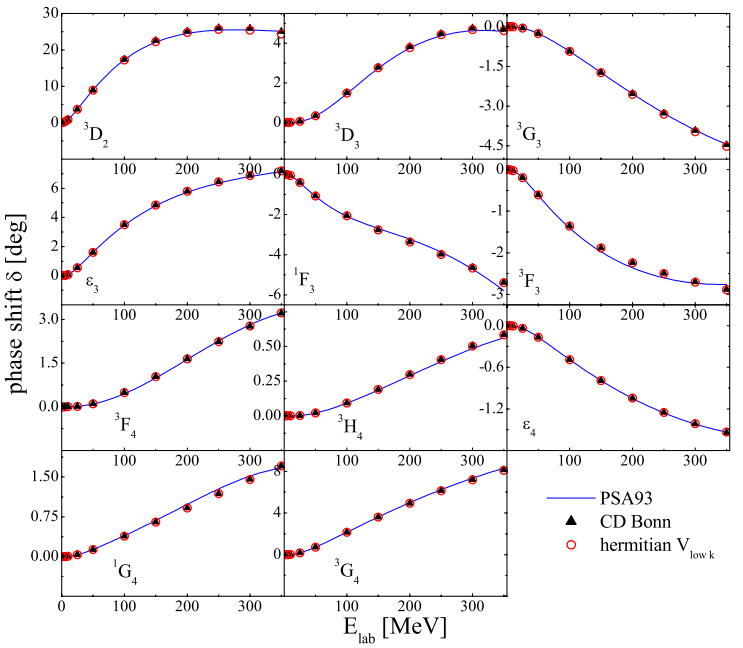

Fig. 17. The neutron–proton phase shifts and mixing parameters are continued from Fig. 16, for details we refer to the text of Fig. 16.

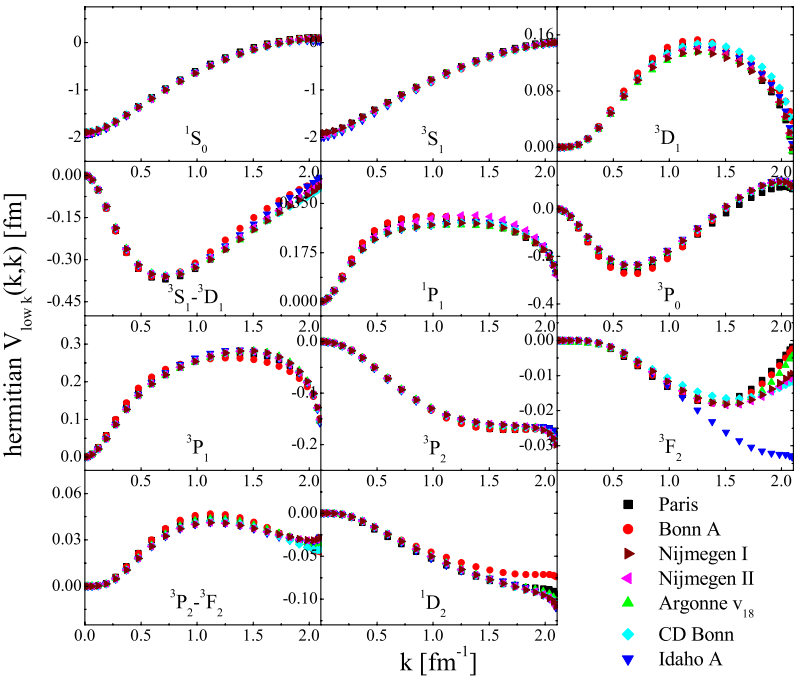

Fig. 18. Diagonal momentum-space matrix elements of the hermitian $\bar{V}_{\mathrm{low}\,k}$ obtained from the different potential models for a cutoff $\Lambda = 2.1$ fm^{-1}. Results are shown for the partial waves $J \leqslant 4$.

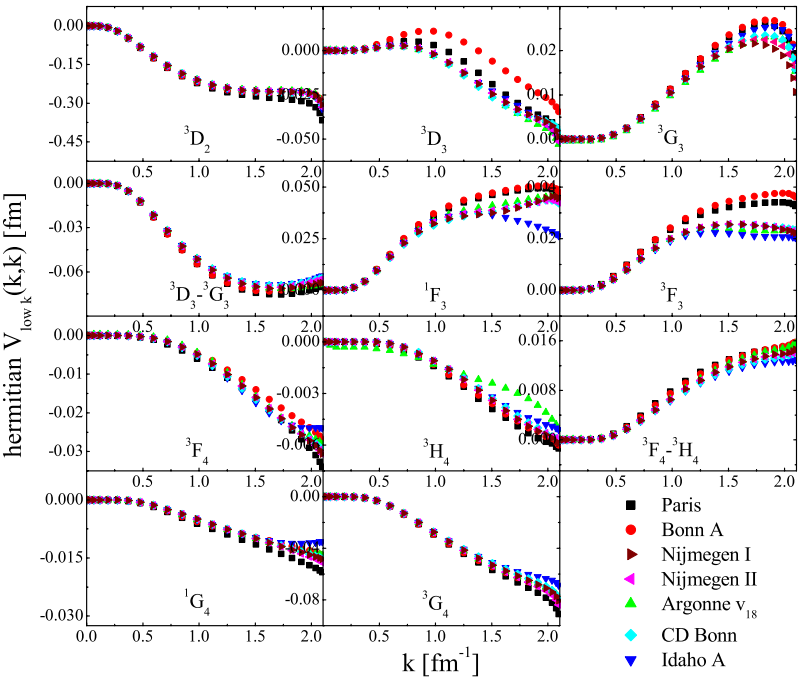

Fig. 19. The diagonal elements of the hermitian $\bar{V}_{\mathrm{low}\,k}$ are continued from Fig. 18.

low momentum nucleons from the ambiguous short-distance parametrizations used in the realistic potential models.

The RG invariance of the effective theory guarantees that the HOS T matrix and the deuteron properties of the full theory are exactly preserved in the model space. Consequently, $V_{\mathrm{low}\,k}$ is phase shift equivalent to the high precision potential models and reproduces the experimental elastic scattering data with similar accuracy. A further refinement transforms $V_{\mathrm{low}\,k}$ into a hermitian low momentum interaction $\bar{V}_{\mathrm{low}\,k}$, which remains model independent and preserves the low-energy on-shell amplitudes of the bare interactions. In this manner, the resulting RG decimation incorporates the model-independent effects of the short-distance physics in the low momentum interaction, while the model-dependent effects are filtered out.

We believe that the low momentum interaction $V_{\mathrm{low}\,k}$ satisfies the first of the two requirements of a microscopic many-body theory given in the Introduction. Namely, that the input interaction is, as best as possible, based on the available low-energy data. A necessary condition for the collapse of the low momentum interactions is the separation of long from short-distance scales in the nuclear problem. In addition, we have argued that the accuracy of the reproduction of the phase shifts drives the collapse of the on-shell components of the low momentum interactions. Furthermore, the evolution of $V_{\mathrm{low}\,k}$ with the cutoff provides physical insight into the separation of scales in the nuclear problem, the effects of the short-range repulsion in the renormalization, and the tensor content of the low momentum interaction.

$V_{\mathrm{low}\,k}$ sums high momentum ladders in free space. Therefore, the low momentum interaction is considerably softer than the bare interactions and does not have a repulsive core. As a consequence, when used as the microscopic input in the many-body problem, $V_{\mathrm{low}\,k}$ does not lead to strong high momentum scattering effects in the particle–particle channel, which necessitates a Brueckner resummation or short-range correlation methods for the conventional models.

The low momentum interaction should be regarded as a new input potential for many-body calculations. However, we emphasize that in contrast to the Brueckner G matrix, $V_{\mathrm{low}\,k}$ does not have high momentum components above the cutoff and therefore one does not have to be concerned about double counting the high momentum contributions. In EFT, this is understood easily, since the ultraviolet divergences can be renormalized in free space and the many-body dynamics does not lead to new ultraviolet divergences. More precisely, in any many-body diagram, the excitations to high momentum states that are absorbed in $V_{\mathrm{low}\,k}$ vanish due to the momentum space cutoff by construction. Using $V_{\mathrm{low}\,k}$ is simply analogous to using the relatively soft CD Bonn interaction, instead of the stronger Argonne v_{18} potential.

Since $V_{\mathrm{low}\,k}$ accounts for a large part of the phase space in the many-body system, it will be interesting to explore whether calculations starting with $V_{\mathrm{low}\,k}$ could be organized in a more perturbative fashion. Encouraging results for a perturbative expansion of the shell model effective Hamiltonian in few-body systems has been demonstrated for the deuteron in [39]. For larger systems, this idea more relies on a geometrical phase space argument.

Acknowledgements

We thank Gerry Brown, Bengt Friman and Dick Furnstahl for helpful discussions. This work was supported by the US-DOE Grant DE-FG02-88ER40388, the US-DOE Grant DE-FG03-00ER41132, the NSF under Grant No. PHY-0098645 and by an Ohio State University Postdoctoral Fellowship.

Appendix

Diagonal matrix elements of the hermitian $\bar{V}_{\text{low } k}$ (see Figs. 18 and 19).

References

[1] S.C. Pieper, V.R. Pandharipande, R.B. Wiringa, J. Carlson, Phys. Rev. C 64 (2001) 014001.
[2] S.C. Pieper, K. Varga, R.B. Wiringa, nucl-th/0206061.
[3] S.K. Bogner, T.T.S. Kuo, L. Coraggio, Nucl. Phys. A 684 (2001) 432c.
[4] S.K. Bogner, T.T.S. Kuo, A. Schwenk, D.R. Entem, R. Machleidt, nucl-th/0108041.
[5] R. Machleidt, I. Slaus, J. Phys. G 27 (2001) R69.
[6] R. Vinh Mau, An advanced course in modern nuclear physics, in: J.M. Arias, M. Lozano (Eds.), Lecture Notes in Physics, Vol. 581, Springer, Berlin, 2001, p. 1.
[7] M. Lacombe, B. Loiseau, J. M. Richard, R. Vinh Mau, J. Côté, P. Pirès, R. de Tourreil, Phys. Rev. C 21 (1980) 861.
[8] R. Machleidt, K. Holinde, C. Elster, Phys. Rep. 149 (1987) 1.
[9] R. Machleidt, F. Sammarruca, Y. Song, Phys. Rev. C 53 (1996) 1483.
[10] R. Machleidt, Phys. Rev. C 63 (2001) 024001.
[11] V.G.J. Stoks, R.A.M. Klomp, C.P.F. Terheggen, J.J. de Swart, Phys. Rev. C 49 (1994) 2950.
[12] R.B. Wiringa, V.G.J. Stoks, R. Schiavilla, Phys. Rev. C 51 (1995) 38.
[13] S. Weinberg, Phys. Lett. B 251 (1990) 288.
[14] S. Weinberg, Nucl. Phys. B 363 (1991) 3.
[15] C. Ordonez, L. Ray, U. van Kolck, Phys. Rev. Lett. 72 (1994) 1982.
[16] D.B. Kaplan, M.J. Savage, M.B. Wise, Nucl. Phys. B 534 (1998) 329.
[17] T.-S. Park, K. Kubodera, D.-P. Min, M. Rho, Phys. Rev. C 58 (1998) 637.
[18] E. Epelbaum, W. Glockle, U.-G. Meissner, Nucl. Phys. A 671 (2000) 295.
[19] D.R. Entem, R. Machleidt, Phys. Lett. B 524 (2001) 93.
[20] S.R. Beane, P.F. Bedaque, W.C. Haxton, D.R. Phillips, M.J. Savage, in: M. Shifman (Ed.), At the Frontier of Particle Physics, Vol. 1, World Scientific, Singapore, p. 133, nucl-th/0008064.
[21] H.A. Bethe, C. Longmire, Phys. Rev. 77 (1950) 647.
[22] G.E. Brown, A.D. Jackson, The Nucleon–Nucleon Interaction, North-Holland, Amsterdam, 1976.
[23] G.P. Lepage, "how to renormalize the Schrödinger equation", Lectures given at 9th Jorge Andre Swieca Summer School: Particles and Fields, Sao Paulo, Brazil, February, 1997, nucl-th/9706029.
[24] V.G.J. Stoks, R.A.M. Klomp, M.C.M. Rentmeester, J.J. de Swart, Phys. Rev. C 48 (1993) 792.
[25] NN-OnLine, http://nn-online.sci.kun.nl.
[26] S.K. Bogner, A. Schwenk, T.T.S. Kuo, G.E. Brown, nucl-th/0111042.
[27] M. Hjorth-Jensen, T.T.S. Kuo, E. Osnes, Phys. Rept. 261 (1995) 125.
[28] C. Bloch, Nucl. Phys. 6 (1958) 329.
[29] C. Bloch, J. Horowitz, Nucl. Phys. 8 (1958) 91.
[30] W.C. Haxton, C.-L. Song, Phys. Rev. Lett. 84 (2000) 5484.
[31] S.Y. Lee, K. Suzuki, Phys. Lett. B 91 (1980) 173.
[32] K. Suzuki, S.Y. Lee, Prog. Theor. Phys. 64 (1980) 2091.
[33] F. Andreozzi, Phys. Rev. C 54 (1996) 684.
[34] K. Suzuki, Prog. Theor. Phys. 68 (1982) 246.
[35] K. Suzuki, R. Okamoto, Prog. Theor. Phys. 70 (1983) 439.
[36] S. Okubo, Prog. Theor. Phys. 12 (1954) 603.
[37] T.T.S. Kuo, S.Y. Lee, K.F. Ratcliff, Nucl. Phys. A 176 (1971) 65.
[38] T.T.S. Kuo, E. Osnes, Folded-diagram theory of the effective interaction in nuclei, atoms and molecules, Lecture Notes in Physics, Vol. 364, Springer, Berlin, 1990, p. 1.
[39] W.C. Haxton, T. Luu, Phys. Rev. Lett. 89 (2002) 182503.